International Journal of Solids and Structures 48 (2011) 3471–3483

Contents lists available at SciVerse ScienceDirect

International Journal of Solids and Structures

journal homepage: www.elsevier.com/locate/ijsolstr

Stretch-induced stress patterns and wrinkles in hyperelastic thin sheets

Vishal Nayyar, K. Ravi-Chandar, Rui Huang *

Department of Aerospace Engineering and Engineering Mechanics, The University of Texas at Austin, Austin, TX 78712, United States

ARTICLE INFO

Article history:
Received 1 July 2011
Received in revised form 1 September 2011
Available online 10 September 2011

Keywords:
Buckling
Wrinkle
Thin sheet
Hyperelastic material

ABSTRACT

Wrinkles are commonly observed in stretched thin sheets and membranes. This paper presents a numerical study on stretch-induced wrinkling of hyperelastic thin sheets based on nonlinear finite element analyses. The model problem is set up for uniaxial stretching of a rectangular sheet with two clamped ends and two free edges. A two-dimensional stress analysis is performed first under the plane-stress condition to determine stretch-induced stress distribution patterns in the elastic sheets, assuming no wrinkles. As a prerequisite for wrinkling, development of compressive stresses in the transverse direction is found to depend on both the length-to-width aspect ratio of the sheet and the applied tensile strain in the longitudinal direction. A phase diagram is constructed with four different distribution patterns of the stretch-induced compressive stresses, spanning a wide range of aspect ratio and tensile strain. Next, an eigenvalue analysis is performed to find the potential buckling modes of the elastic sheet under the prescribed boundary conditions. Finally, a nonlinear post-buckling analysis is performed to show evolution of stretch-induced wrinkles. In addition to the aspect ratio and tensile strain, it is found that the critical condition for wrinkling and the post-buckling behavior both depend sensitively on the sheet thickness. In general, wrinkles form only when both the magnitude and the distribution area of the compressive stresses are sufficiently large. The wrinkle wavelength decreases with increasing strain, in good agreement with the prediction by a scaling analysis. However, as the tensile strain increases, the wrinkle amplitude first increases and then decreases, eventually flattened beyond a moderately large critical strain, in contrast to the scaling analysis.

1. Introduction

Thin sheets and membrane structures are used widely in space applications such as inflatable space antennas, solar sails, and radars (Talley et al., 2002; Sleight et al., 2005; Sakamoto and Park, 2005; Wang et al., 2007). Similar structures have also found applications in areas of solar energy systems (Peypoudat et al., 2005) and large-area flexible electronics (Rogers et al., 2001). The main advantage of using these structures in the space applications is due to their lightweight and low space requirement. Among others, surface flatness over a large area is one of the key requirements for many applications using the flexible thin structures (Wang et al., 2007). For instance, in a solar sail, surface wrinkles may lead to problems such as non-uniform sail loading, loss of momentum transfer to sail, and undesirable torques on the spacecraft (Talley et al., 2002). Typically, wrinkles form as a result of structural instability under compressive stresses. However, previous studies have shown that wrinkles often appear in thin sheets under a variety of loading conditions (Jenkins et al., 1998; Su et al., 2003; Leifer and Belvin, 2003; Wong and Pellegrino, 2006a). It is thus important to understand the mechanics of wrinkling for practical applications that require reliable control of surface wrinkles.

Two approaches have been commonly used for wrinkling analysis of elastic membranes: the tension field theory and the bifurcation analysis. In the tension field theory, the membrane is assumed to have zero bending stiffness. This approach was first applied by Wagner (1929) to estimate the maximum shear load that can be carried by a thin web. Stein and Hedgepeth (1961) adopted the approach in analysis of partly wrinkled membranes, where a wrinkling region is assumed whenever one of the in-plane principal stresses becomes negative. Subsequently, the tension field theory has been continuously developed and extended for various applications (e.g., Mansfield, 1970; Danielson and Natarajan, 1975; Wu, 1978; Pipkin, 1986; Steigmann, 1990; Alder et al., 2000; Liu et al., 2001; Coman, 2007). The tension field theory approach typically provides a satisfactory prediction of the stress distribution and wrinkling regions. However, it does not provide detailed information about the wrinkles such as amplitude and wavelength.

In the bifurcation analysis, the membrane is treated as a thin shell with non-zero bending stiffness. Typically, a geometrically nonlinear finite element method is employed using shell elements for numerical analysis (e.g., Tomita and Shindo, 1988; Friedl et al.,

* Corresponding author.
E-mail address: ruihuang@mail.utexas.edu (R. Huang).

0020-7683/$ - see front matter © 2011 Elsevier Ltd. All rights reserved.
doi:10.1016/j.ijsolstr.2011.09.004

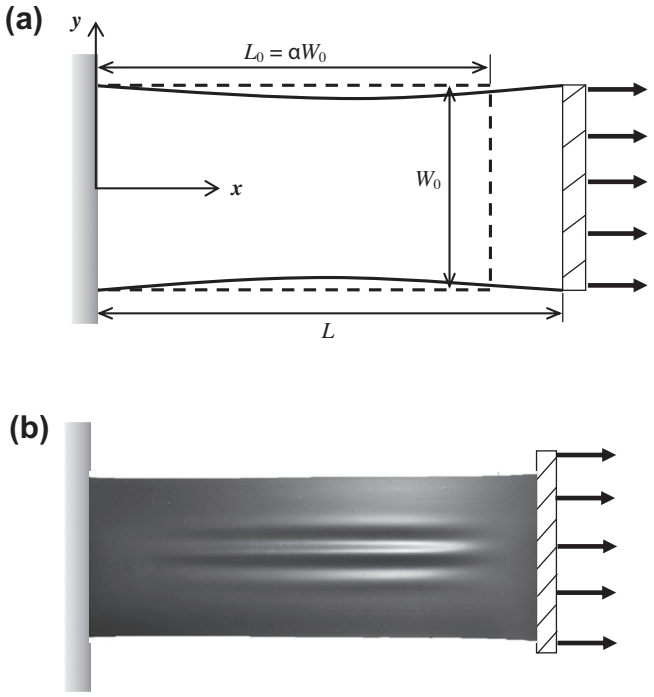

Fig. 1. (a) Schematic illustration of a rectangular sheet with two clamped-ends, subject to uniaxial stretch. (b) An optical image of a wrinkled polyethylene sheet under stretch ($\varepsilon \sim 10\%$).

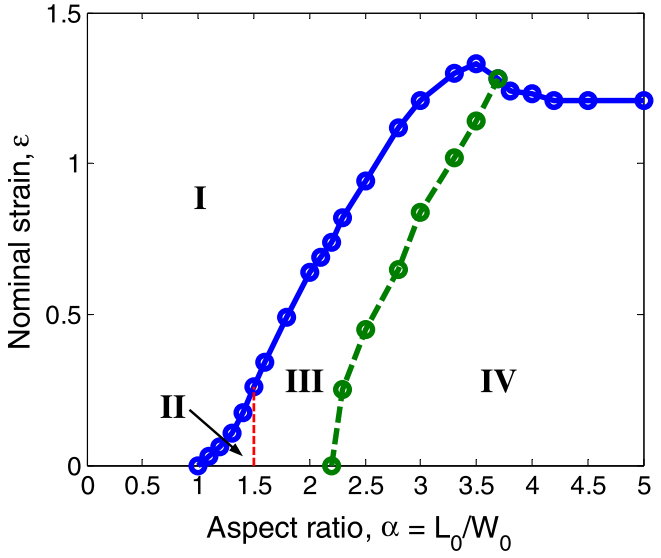

Fig. 2. A phase diagram for stretch-induced compressive stress patterns in end-clamped rectangular sheets.

2000; Lee and Lee, 2002; Leifer and Belvin, 2003; Iwasa et al., 2004; Tessler et al., 2005; Wong and Pellegrino, 2006c; Diaby et al., 2006; Zheng, 2009). Both the critical condition for wrinkling and post-buckling behavior can be predicted by this approach. For relatively simple cases, analytical methods have also been proposed to obtain approximate solutions (Jacques and Potier-Ferry, 2005; Wong and Pellegrino, 2006b; Coman and Haughton, 2006; Steigmann, 2008; Puntel et al., 2011).

In the present study we take the approach of bifurcation analysis and focus on a model problem as depicted in Fig. 1a: a rectangular sheet is subjected to uniaxial stretch with two opposite ends clamped. Fig. 1b shows an image of a stretched polyethylene sheet with wrinkles. The same problem has been studied previously. Friedl et al. (2000) showed that compressive transverse stresses are induced in the sheet upon stretching as a result of the clamped boundary condition. They suggested a buckling coefficient to determine the critical longitudinal stress for onset of wrinkling. Jacques and Potier-Ferry (2005) presented an analytical solution to explain the wrinkle wavelength selection and mode localization in relatively long sheets. Cerda et al. (2002) presented the first experimental data for stretch-induced wrinkle wavelengths along with a scaling analysis, which predicted the wavelength to decrease with increasing longitudinal strain while the wrinkle amplitude increases. Cerda and Mahadevan (2003) later extended the scaling analysis for a wide range of wrinkling phenomena. Recently, with a more elaborate analysis, Puntel et al. (2011) confirmed the scaling relation for the wrinkle wavelength but showed that wrinkling occurs only beyond a critical stretch, which depends on the length-to-width ratio of the rectangular sheet. Zheng (2009) presented both numerical analyses and experimental measurements of the wrinkles, showing that the wrinkle amplitude first increases and then decreases as the longitudinal strain increases. All of the previous studies except for Zheng (2009) assumed the material of the sheet to be linear elastic, which restricts the longitudinal strain to be less than a few percent. In the present study, to consider moderately large strains (up to 150%), the material is taken to be hyperelastic. Unlike Zheng (2009), we start with a two-dimensional analysis of stress distribution in the sheet (Section 2), which predicts various patterns of stretch-induced compressive stresses for the rectangular sheets with different length-to-width aspect ratios. Subsequently, we present critical eigenvalue analyses for onset of buckling modes (Section 3) and nonlinear post-buckling analyses for evolution of stretch-induced wrinkles (Section 4). Furthermore, a simple model is presented to qualitatively understand the numerical results.

2. Two-dimensional stress analysis

Fig. 1a shows schematically a rectangular sheet, subjected to uniaxial stretch in the longitudinal direction with two opposite ends clamped. Before stretching, the dimensions of the sheet are: length L_0, width W_0, and thickness t_0. The nominal strain is defined as $\varepsilon = L/L_0 - 1$, where L is the end-to-end distance of the stretched sheet. Due to the constraint of the clamped ends, the deformation and stress in the sheet are inhomogeneous. In this section, we present a two-dimensional (2-D) stress analysis of the stretched sheet, assuming no wrinkles. A 2-D finite element model is developed using the commercial software ABAQUS (v6.8, 2008), where the sheet is modeled by quadrilateral plane-stress elements (CPS4R). A uniform mesh is used with 100 nearly square-shaped elements across the width of the sheet, which was found sufficient to achieve convergence in the 2-D stress analysis (Nayyar, 2010). The geometry of the rectangular sheet is characterized by a single dimensionless ratio between the length and the width, $\alpha = L_0/W_0$. The thickness of the sheet has no effect on the 2-D stress analysis, but will be important for wrinkling analysis in later sections. The material of the sheet is assumed to be hyperelastic so that moderately large deformation can be considered. Using the incompressible neo-Hookean model for the material, the only material property to be specified is the initial shear modulus (μ). To be specific, we set $\mu = 6$ MPa, a representative value for rubberlike materials. The value of the shear modulus affects only the magnitude of stress in the sheet but has no effect on the wrinkling behavior as shown later. In addition to the nonlinear elasticity of the material, the nonlinear kinematics for finite deformation is taken into account in the finite element analysis.

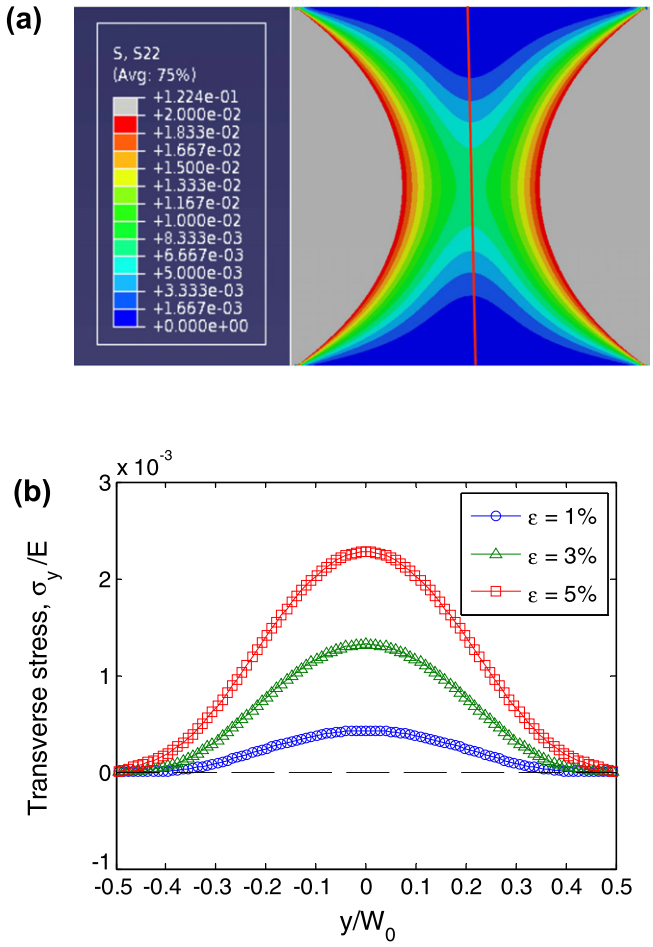

Fig. 3. (a) Contour plots of the stretch-induced transverse stress (σ_y) for $\alpha = 1$ and $\varepsilon = 1\%$, showing no compressive stress; (b) Distribution of the transverse stress along the vertical center line of the sheet under different strains.

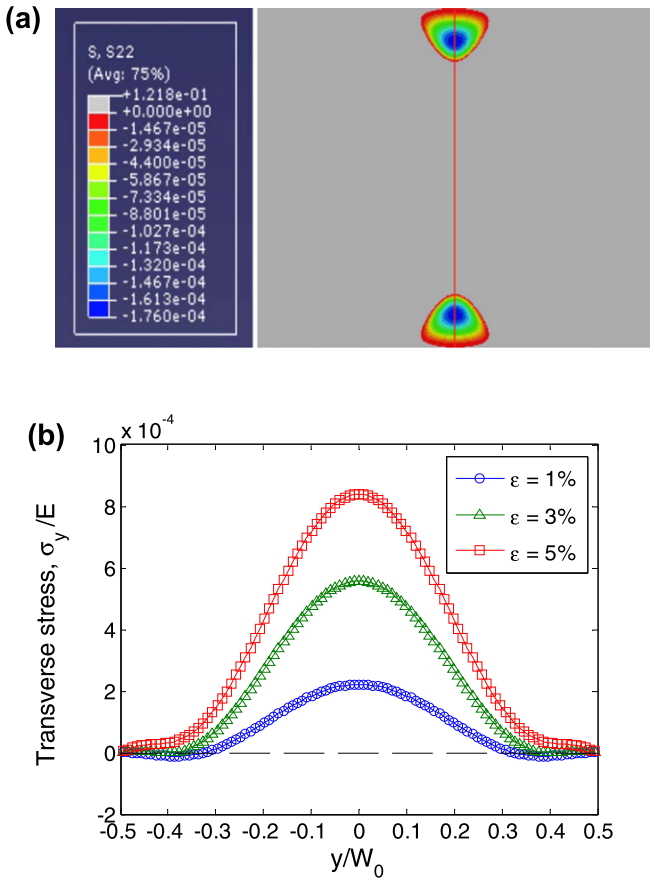

Fig. 4. (a) Contour plots of stretch-induced transverse stress (σ_y) for $\alpha = 1.1$ and $\varepsilon = 1\%$, showing the compressive stress in two separate regions; (b) Distribution of the transverse stress along the vertical center line of the sheet under different strains.

To understand the effect of the aspect ratio ($\alpha = L_0/W_0$), we vary the initial length (L_0) of the sheet while keeping the width constant ($W_0 = 10$ cm, to be specific) in all models. For each aspect ratio, the sheet is increasingly stretched by prescribing the end displacements, up to a moderately large nominal strain ($\varepsilon \leqslant 150\%$). It is found that for a wide range of the aspect ratio compressive stresses are induced in the transverse direction of the sheet (i.e., $\sigma_y < 0$), which is a prerequisite for wrinkling. In addition, different distribution patterns of the stretch-induced compressive stress are predicted, depending on the aspect ratio and the applied stretch. Fig. 2 summarizes the results in a phase diagram for the stress patterns, including four different phases: (I) all-tension phase (see Fig. 3); (II) transverse two-peak phase (see Figs. 4 and 5); (III) central one-peak phase (see Fig. 6); (IV) longitudinal two-peak phase (see Figs. 7 and 8). The details are discussed as follows.

2.1. Case 1: low aspect ratio ($\alpha \leqslant 1$)

For rectangular sheets with low aspect ratios ($\alpha \leqslant 1$), no compressive stress is induced by stretching the sheets with the prescribed boundary condition. Fig. 3a shows the stress contour (σ_y) for a sheet with $\alpha = 1$ and $\varepsilon = 1\%$, where the stress magnitude is normalized by Young's modulus of the material ($E = 3\mu$). The entire sheet is under tension in both the x and y directions; consequently, no wrinkling is expected in this case. We note that the resolution of the singular stress field at the corners (Benthem, 1963) may require use of a very fine mesh or singular elements in the finite element model. However, for the discussion of stretch-induced wrinkling, only the stress distribution away from the corners is of importance and thus a moderately fine mesh is sufficient. Due to the constraint of uniaxial strain at the clamped ends (i.e., zero strain in the y-direction), a biaxial tensile stress field develops near the ends. However, due to the two free edges at $y/W_0 = \pm 0.5$, the tensile stress in the y direction is partially relaxed in the center region of the sheet, but remains tensile everywhere for the low-aspect-ratio sheet. Fig. 3b shows the transverse stress σ_y along the vertical center line of the sheet ($x/L_0 = 0.5$). The stress σ_y is necessarily zero at the edge ($y/W_0 = \pm 0.5$) by the boundary condition. Away from the edges, σ_y increases and reaches a peak at the center of the sheet ($y = 0$). As the nominal strain increases, the magnitude of the tensile transverse stress increases. Therefore, regardless of the applied stretch, the stress field is completely tensile for the low-aspect-ratio sheets; this is designated as Phase I in Fig. 2.

2.2. Case 2: $1 < \alpha < 1.5$

With the aspect ratio slightly greater than 1, a compressive stress is induced in the rectangular sheet upon stretching. As shown in Fig. 4a for $\alpha = 1.1$ and $\varepsilon = 1\%$, the stress σ_y is negative in two separate regions symmetrically located near the free edges, with two peak compressive stresses on the vertical center line. As shown in Fig. 4b, at $\varepsilon = 1\%$ the transverse stress along the center line is compressive near the edges and tensile at the center. As the applied strain increases, the magnitude of the compressive stress first increases and then decreases, becoming all tensile at $\varepsilon = 5\%$. Therefore, for such an aspect ratio, a two-peak compressive stress pattern is induced at small strains; this is designated as Phase II in

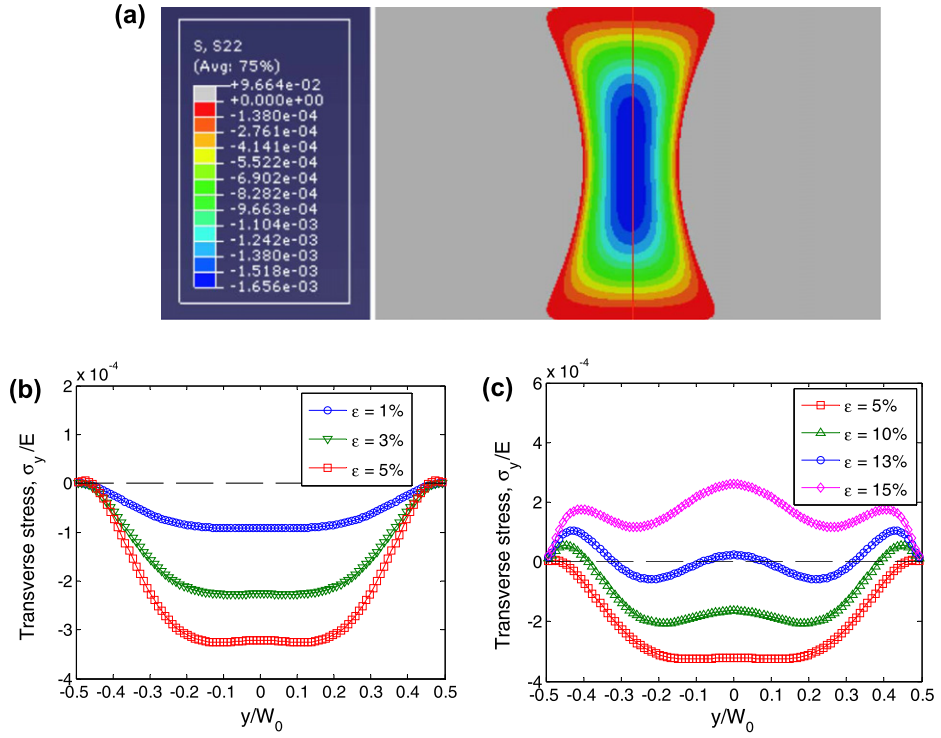

Fig. 5. (a) Contour plots of stretch-induced transverse stress (σ_y) for $\alpha = 1.35$ and $\varepsilon = 1\%$, showing only the compressive stress region; (b) and (c) Distributions of the transverse stress along the vertical center line of the sheet under increasing nominal strains.

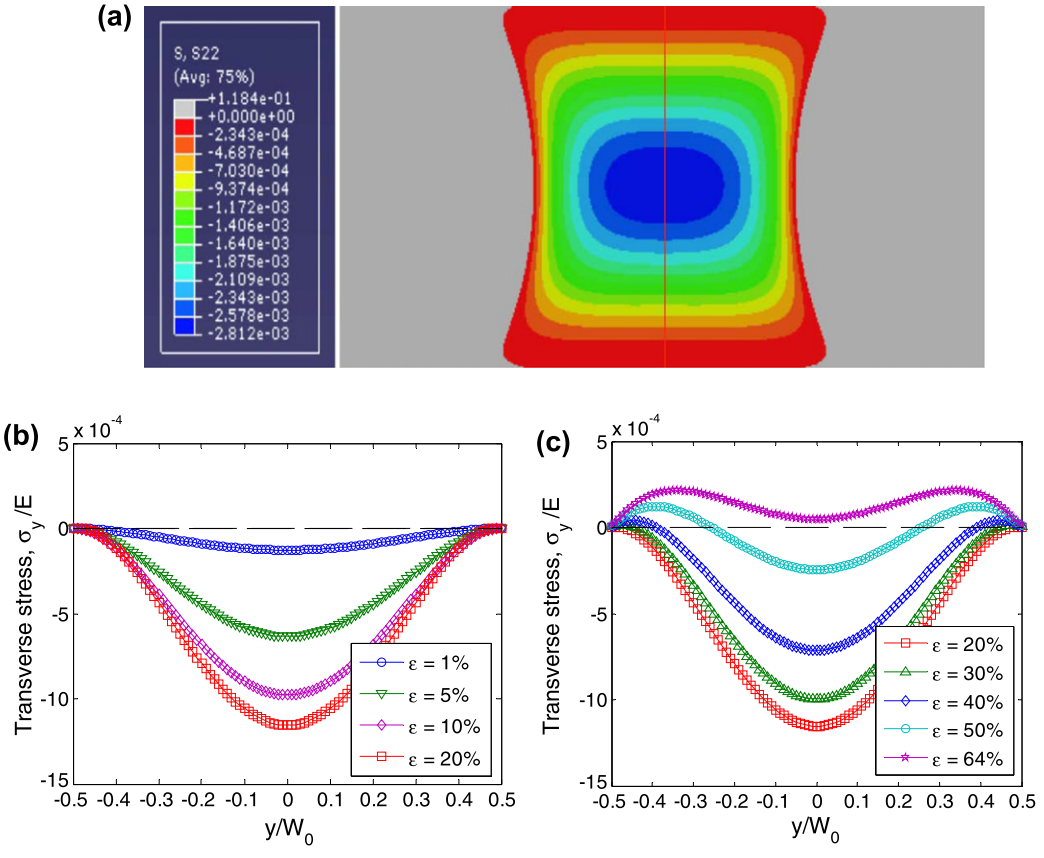

Fig. 6. (a) Contour plots of stretch-induced transverse stress (σ_y) for $\alpha = 2$ and $\varepsilon = 1\%$, showing only the compressive stress region; (b) and (c) Distributions of the transverse stress along the vertical center line of the sheet under increasing nominal strains.

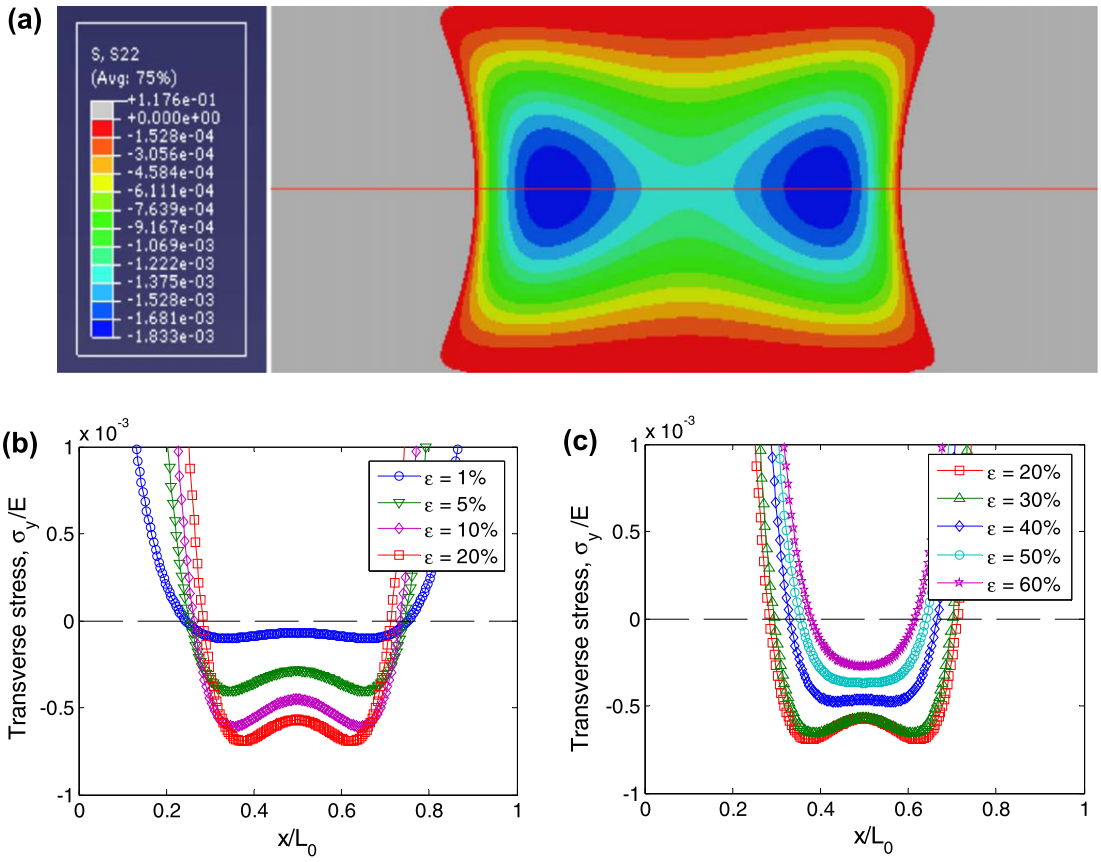

Fig. 7. (a) Contour plots of stretch-induced transverse stress (σ_y) for $\alpha = 2.5$ and $\varepsilon = 1\%$, showing only the compressive stress region; (b) and (c) Distributions of the transverse stress along the horizontal center line of the sheet under increasing nominal strains.

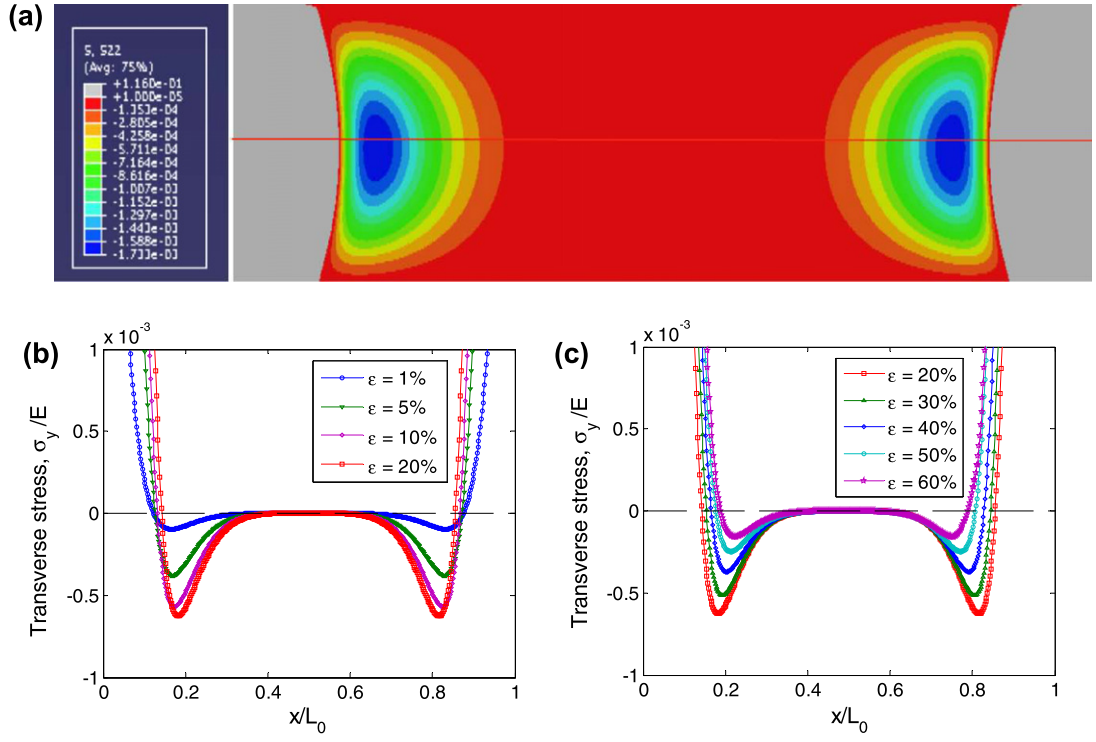

Fig. 8. (a) Contour plots of stretch-induced transverse stress (σ_y) for $\alpha = 5$ and $\varepsilon = 1\%$, showing only the compressive stress region; (b) and (c) Distributions of the transverse stress along the horizontal center line of the sheet under increasing nominal strains.

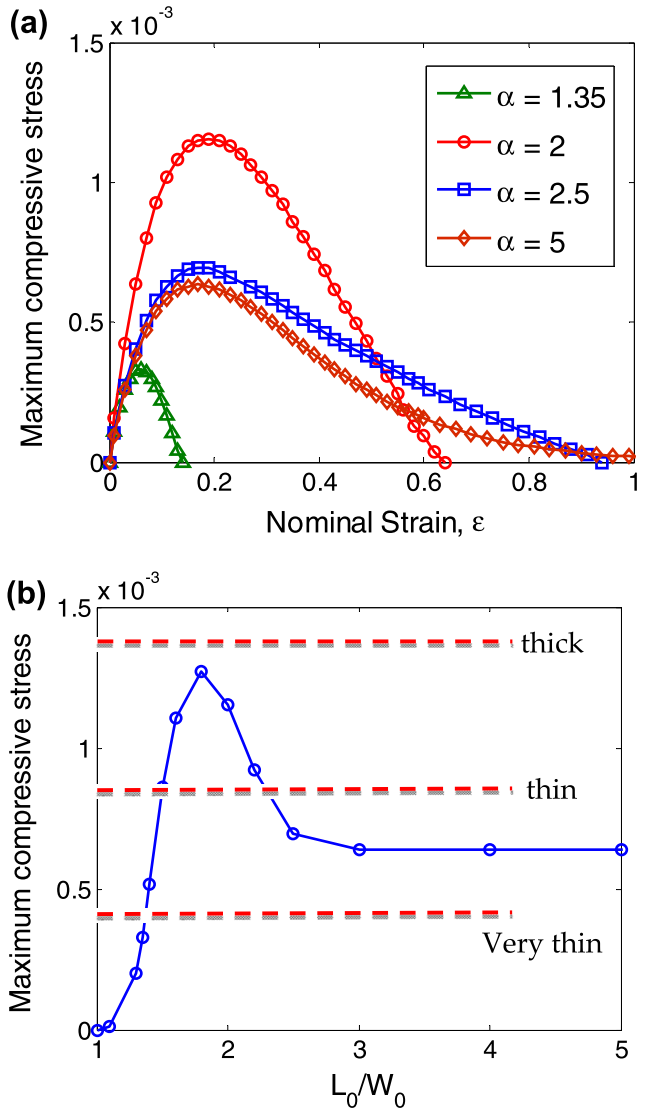

Fig. 9. (a) Variation of the maximum compressive stress magnitude in the rectangular sheets under increasing stretch for different aspect ratios; (b) Maximum magnitude of the stretch-induced compressive stress as a function of the aspect ratio. Dashed lines indicate the critical buckling stresses for different sheet thicknesses.

Fig. 2. A transition from Phase II to Phase I (all-tension) occurs at a critical strain that increases with the aspect ratio.

For aspect ratios up to 1.5, the distribution of the stretch-induced compressive stress exhibits similar pattern, with two peaks along the vertical center line of the sheet. As the aspect ratio increases, the locations of the two peaks move toward the center. Meanwhile, the two regions of the compressive stress expand and eventually merge into one region from edge to edge, as shown in Fig. 5a for $\alpha = 1.35$ and $\varepsilon = 1\%$. With increasing stretch, the magnitude of the compressive stress first increases (Fig. 5b) and then decreases (Fig. 5c), becoming all tension at $\varepsilon = 15\%$.

The boundary between Phase I and Phase II in Fig. 2 is determined approximately from the finite element analysis. First, the critical aspect ratio between the two phases is found to be around 1. Second, for $1 < \alpha < 1.5$, the critical strain for the transition from Phase II to Phase I is calculated as a function of the aspect ratio. At $\alpha = 1.5$, it is found that the two peaks of the compressive stress merge into one at the center of the sheet ($y = 0$ and $x/L_0 = 0.5$); this is designated as Phase III in Fig. 2.

2.3. Case 3: $1.5 \leqslant \alpha < 2.2$

For $1.5 \leqslant \alpha < 2.2$, a region of compressive stress develops at the center of the rectangular sheet upon stretching, with the peak compressive stress at the center of symmetry ($y = 0$ and $x/L_0 = 0.5$), as shown in Fig. 6a for $\alpha = 2$ and $\varepsilon = 1\%$. The one-peak distribution pattern is designated as Phase III in Fig. 2. Friedl et al. (2000) showed a similar stress pattern for a linear elastic sheet with $\alpha = 2$. Along the vertical center line of the sheet, the stress σ_y is compressive from edge to edge for $\varepsilon < 20\%$. The magnitude of the peak compressive stress first increases as the applied stretch increases up to $\varepsilon = 20\%$, as shown in Fig. 6b. As the applied stretch increases further, the stress becomes tensile near the edges and the magnitude of the peak compressive stress at the center decreases (Fig. 6c). Eventually at $\varepsilon = 64\%$, the stress becomes all tension (Phase I) again. Similar to the transition from Phase II to Phase I, the critical strain for the transition from Phase III to Phase I increases as the aspect ratio increases, which defines the boundary between Phase III and Phase I in Fig. 2.

2.4. Case 4: $2.2 \leqslant \alpha < 3.7$

As the aspect ratio continues to increase, the region of the stretch-induced compressive stress expands in the x direction. When $\alpha \geqslant 2.2$, the peak compressive stress at the center splits into two peaks symmetrically located on the x-axis, as shown in Fig. 7a for $\alpha = 2.5$ and $\varepsilon = 1\%$. The longitudinal two-peak distribution of the stretch-induced compressive stress is designated as Phase IV in Fig. 2. Fig. 7b shows the transverse stress (σ_y) along the x-axis (horizontal center line of the sheet) for $\alpha = 2.5$. The stress is tensile near the clamped ends, but becomes compressive approaching the center of the sheet. The magnitude of the peak compressive stress increases with increasing stretch up to $\varepsilon = 20\%$. Further increasing the stretch, the magnitude of the peak compressive stress decreases, as shown in Fig. 7c. Meanwhile, the location of the peak compressive stress moves towards the center as the stretch increases. At $\varepsilon = 60\%$, the two peaks merge into one at the center of the sheet. Therefore, the distribution pattern of the stretch-induced compressive stress changes from Phase IV to Phase III. As shown in Fig. 2, the critical strain for this transition increases with the aspect ratio for $2.2 \leqslant \alpha < 3.7$. As the applied stretch continues to increase, a transition from Phase III to Phase I (all-tension) occurs, similar to that shown in Fig. 6 for Case 3.

2.5. Case 5: high aspect ratio ($\alpha \geqslant 3.7$)

For rectangular sheets with the length-to-width aspect ratio greater than 3.7, the stretch-induced compressive stress has two peaks symmetrically located on the x-axis (Phase IV) when the applied stretch is less than a critical strain. Beyond the critical strain, the stress distribution becomes all tension (Phase I). Unlike in Case 4, the stress pattern transitions directly from Phase IV to Phase I, without going through Phase III. As shown in Fig. 2, the critical strain for this transition is nearly independent of the aspect ratio.

With a high aspect ratio, the two peaks of the compressive stress are located far apart from each other, and the region of compressive stress is split into two separate regions, with nearly zero σ_y at the center region of the sheet, as shown in Fig. 8a for $\alpha = 5$ and $\varepsilon = 1\%$. Thus, the stretch-induced compressive stress is localized near the clamped ends. In between, the stress state is essentially uniaxial. Indeed, at the limiting case with $\alpha \gg 1$, it is expected that most part of the sheet is under uniaxial tension with a uniform stress distribution ($\sigma_y = 0$ and $\sigma_x > 0$) except for the regions near the clamped ends. A similar stress pattern was predicted by Friedl et al. (2000) for $\alpha = 7$ and by Benthem (1963) for a semi-infinite strip, both assuming linear elastic properties of

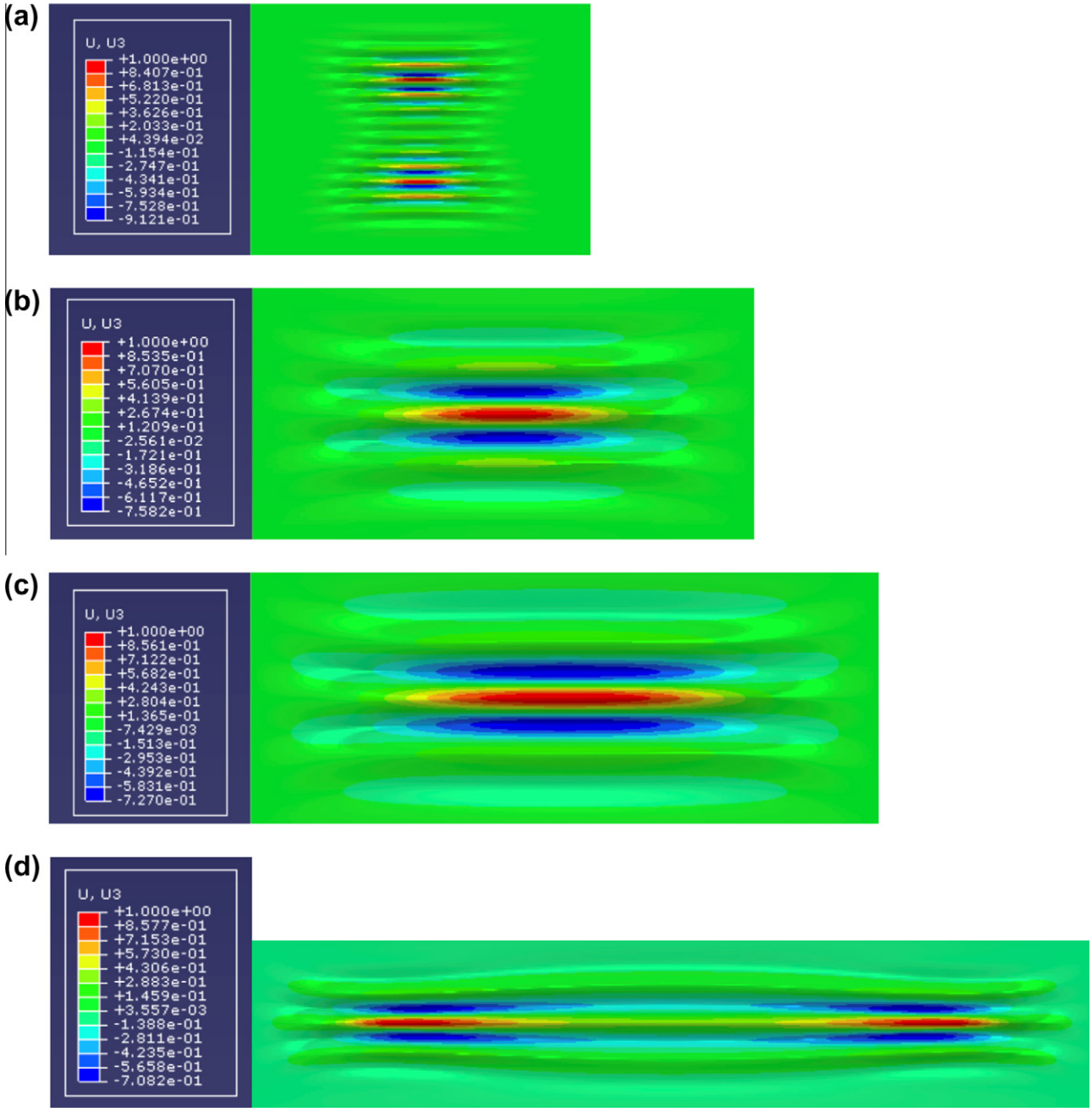

Fig. 10. The first eigenmode for end-clamped rectangular sheets with 1% pre-stretch, obtained from eigenvalue analysis for different aspect ratios. (a) $\alpha = 1.35$; (b) $\alpha = 2$; (c) $\alpha = 2.5$; (d) $\alpha = 5$.

the material. As the applied stretch increases, the locations of the peak compressive stress move towards the center of the sheet, but remain separated. The magnitude of the peak compressive stress first increases (Fig. 8b) and then decreases (Fig. 8c). Eventually, with the nominal strain beyond 130%, the stress distribution becomes all tension (Phase I). Since the two regions of compressive stress are separate with negligible interaction, the behavior becomes independent of the length (L_0) for the rectangular sheets with high aspect ratios.

To summarize the 2-D stress analyses, we plot in Fig. 9a the magnitude of the peak compressive stress as a function of the nominal strain for the rectangular sheets with four different aspect ratios. For all cases with $\alpha > 1$, the magnitude of the peak compressive stress first increases with the nominal strain and then decreases, with a maximum magnitude at an intermediate strain. The maximum magnitude of the peak compressive stress increases with the aspect ratio for $1 < \alpha < 1.8$, but decreases for $\alpha > 1.8$, as shown in Fig. 9b. It may be understood that the magnitude of the peak compressive stress increases as the two peaks on the vertical center line (Phase II) merge into one (Phase III) and decreases as the peak split into two on the horizontal center line (Phase IV). In the case of high aspect ratios ($\alpha > 3.7$), the peak compressive stress and its dependence on the nominal strain becomes essentially independent of the aspect ratio; this can be understood to be the result of separation of the two regions with localized compressive stress near the clamped ends. As shown in Fig. 2, the critical strain for the sheet to become all tension (Phase I) increases with the aspect ratio, with a small overshoot before it saturates at a constant strain ($\sim$130%) for high aspect ratios ($\alpha \geqslant 4$). As discussed above, several types of phase transition for the distribution

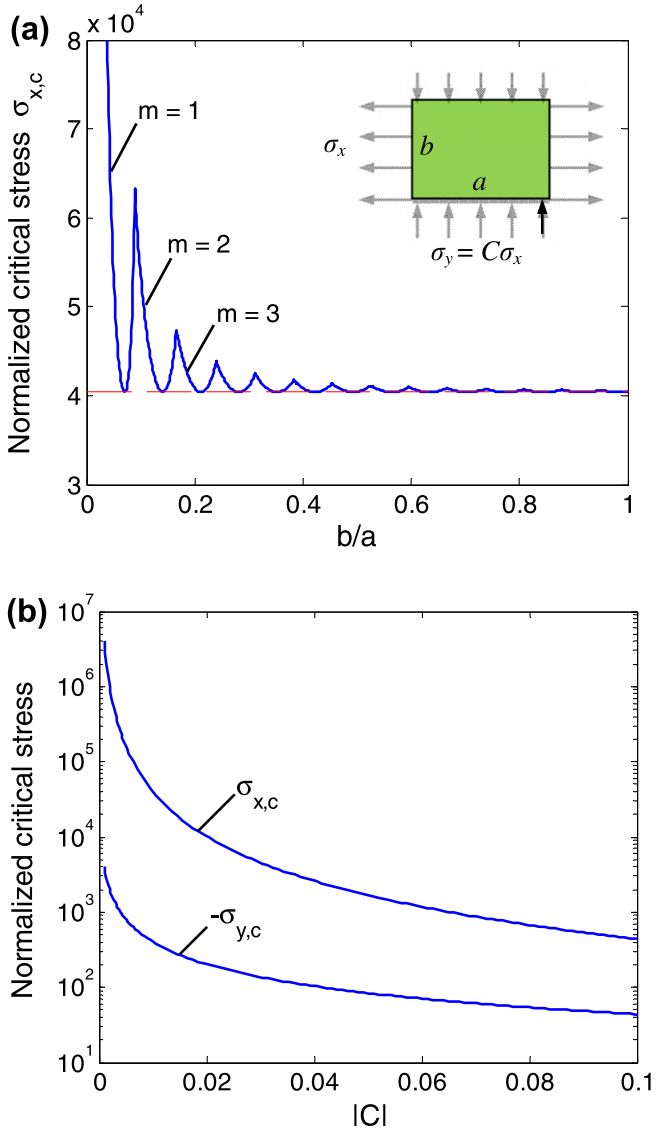

Fig. 11. The critical stress for a simply supported rectangular plate: (a) dependence on the ratio b/a for $C = -0.01$; (b) dependence on the ratio C for relatively large b/a. The stress magnitude is normalized by $\frac{\pi^2 E}{12(1-\nu^2)}\left(\frac{t}{a}\right)^2$. The dashed line in (a) indicates the minimum critical stress given by Eq. (3).

patterns of stretch-induced compressive stress (σ_y) can be observed in the diagram (Fig. 2), including II-to-I, III-to-I, IV-to-III, and IV-to-I.

We close this section by noting two necessary conditions to have stretch-induced compressive stresses in the rectangular sheets. The first condition is the coupling between the longitudinal and transverse deformation, and the second is the constraint due to the clamped ends. In the present study, the longitudinal-transverse coupling arises from the incompressibility of the hyperelastic material model. Similar results were obtained by Friedl et al. (2000) using a linear elastic material model with Poisson's ratio $\nu = 0.3$. On the other hand, if $\nu = 0$, no compressive stress would be induced, regardless of the aspect ratio or the applied strain and hence, no wrinkles would form in the stretched sheet. Alternatively, if the constraint at the clamped ends is relaxed (e.g., allowing end displacement in the transverse direction), a uniaxial tensile stress in the longitudinal direction would be expected with zero transverse stress and hence no wrinkles either.

3. Eigenvalue buckling analysis

To determine whether the stretch-induced compressive stress is sufficient to cause wrinkling of the sheet, we perform an eigenvalue buckling analysis for pre-stretched sheets in this section, followed by a nonlinear post-buckling analysis in Section 4. In addition to the length-to-width aspect ratio, the thickness of the sheet becomes important in both the eigenvalue and post-buckling analyses. In the present study, we take the initial width-to-thickness ratio (W_0/t_0) of the sheet to be 1000. For such a thin sheet, the shell elements (S4R) in ABAQUS are used in the finite element analyses to allow three-dimensional deformation of the sheet. A uniform mesh similar to the 2-D stress analysis is used for the buckling analysis. It is confirmed that when the out-of-plane displacement is numerically suppressed, the finite element model with the shell elements correctly reproduces the stress patterns obtained from the 2-D model with the plane-stress elements in Section 2 (Nayyar, 2010).

To obtain the relevant eigenmodes for stretch-induced wrinkling, a small pre-stretch of 1% is applied in the longitudinal direction before the eigenvalue analysis. For the length-to-width aspect ratio $\alpha < 1.35$, no buckling mode with positive eigenvalues can be found under the prescribed boundary condition. While the stretch-induced compressive stress is present for $1 < \alpha < 1.35$, the magnitude of the compressive stress is low and it is distributed in two small regions as shown in Fig. 4a for $\alpha = 1.1$. In general, both the magnitude and the area of the compressive stresses must be sufficiently large to cause buckling. For $\alpha \geqslant 1.35$, a number of eigenmodes are obtained for the pre-stretched sheet. Fig. 10 shows the first eigenmode for four different aspect ratios. We note the correlation between the buckling mode shapes and the compressive stress patterns in Figs. 5–8. In particular, the transition of the compressive stress pattern from Phase II to III and eventually to IV with increasing aspect ratio is faithfully replicated in the eigenmodes. For $\alpha = 2.5$, however, the eigenmode shows apparently a single peak in the center of the sheet, while the compressive stress has two peaks on the longitudinal axis (Fig. 7). This may be attributed to the close proximity of the two peaks in the compressive stress pattern. When the two peaks are sufficiently separated, the eigenmode shows two peaks as well with a relatively flat region in between, as shown in Fig. 10d for $\alpha = 5$.

It should be pointed out that the results from the eigenvalue analysis, including both the eigenmodes and the corresponding eigenvalues, depends sensitively on the width-to-thickness ratio (W_0/t_0) of the sheet as well as the applied pre-stretch. For the present study, we focus on the eigenmodes at a small pre-stretch (1%), which will be used as geometric imperfections in the post-buckling analysis. Due to nonlinearity in both the material behavior and the kinematics, the eigenvalues do not necessarily predict the critical strain for onset of buckling. Instead, the critical strain will be determined based on the nonlinear post-buckling analysis in Section 4. Alternatively, it is possible to perform the eigenvalue analysis at increasingly large pre-stretch, based on which the critical strain may be determined by noting the first eigenvalue as a function of the pre-stretch, that is, the first eigenvalue would be nearly zero at the critical strain.

A simplified model was suggested by Friedl et al. (2000) to estimate the critical stress for wrinkling. Consider a simply supported rectangular plate subject to a uniform biaxial stress with tension in the x direction and compression in the y direction (see the inset of Fig. 11a). The stress magnitudes are assumed to be proportional, e.g.,

$$\frac{\sigma_y}{\sigma_x} = C < 0. \tag{1}$$

The critical longitudinal stress for buckling of such a plate is (Timoshenko and Gere, 1985)

$$\sigma_{x,c} = \frac{\pi^2 E}{12(1-\nu^2)}\left(\frac{t}{b}\right)^2\left[\frac{n^4\left(\frac{b}{a}\right)^4 + 2m^2n^2\left(\frac{b}{a}\right)^2 + m^4}{-Cm^2 - n^2\left(\frac{b}{a}\right)^2}\right], \tag{2}$$

where the material is assumed to be linear elastic with Young's modulus E and Poisson's ratio ν, n and m are the numbers of half waves in the x and y directions, respectively. The dimensions of the plate are: length a, width b, and thickness t. For $\sigma_x > 0$ and $C < 0$, the critical stress in (2) is minimized with $n = 1$ while m varies with the ratio b/a, as shown in Fig. 11a.

As an approximate model, Eq. (2) may be used to qualitatively understand the onset of stretch-induced wrinkling and the wrinkling modes as well as how they depend on the aspect ratio and the stretch. While Friedl et al. (2000) assumed the simply supported plate to have the same dimensions as the end-clamped sheet, we take the plate approximately to be part of the sheet where the transverse stress (σ_y) is compressive. Therefore, both the length and the width of the plate (a and b) vary with the aspect ratio of the original sheet and with the applied strain. The aspect ratio of the plate (b/a) may be estimated from the stress patterns in Figs. 4–8 as a function of the aspect ratio. In addition, the stress ratio C also depends on the aspect ratio and the strain in general. The stress ratio C may be estimated from Fig. 9a as a function of the nominal strain for each aspect ratio.

Taking the stress ratio approximately to be a constant ($C = -0.01$), the critical stress as predicted by Eq. (2) is plotted in Fig. 11a as a function of the aspect ratio b/a. The number of half waves in the transverse direction (m) increases as b/a increases, qualitatively consistent with the eigenmodes shown in Fig. 10. Note that the aspect ratio b/a for the region of compressive transverse stress in the end-clamped sheet is larger for $\alpha = 1.35$ (Fig. 5) than for $\alpha = 2$ (Fig. 6). As a result, the number of wrinkles in the eigenmode for $\alpha = 1.35$ (Fig. 10a) is greater than for $\alpha = 2$ (Fig. 10b). For a rectangular sheet of high aspect ratio ($\alpha > 3.7$), as the stretch-induced compressive stress splits into two regions, the ratio b/a for each region becomes independent of the aspect ratio α. However, as shown in Fig. 10d for $\alpha = 5$, the wrinkles extend beyond the region of compressive stress, which apparently violates the boundary condition assumed in the simplified model.

For each m, the critical stress in Eq. (2) is minimized for a particular ratio b/a. It can be shown that the minimum critical stress is independent of m, as indicated by the horizontal dashed line in Fig. 11a. For relatively large b/a ($\sim$1), the critical stress for onset of wrinkling depends weakly on the aspect ratio, which is approximately equal to the minimum critical stress, namely

$$\sigma_{x,c} \approx \frac{\pi^2 E}{3(1-\nu^2)}\left(\frac{t}{a}\right)^2\left(\frac{1-C}{C^2}\right). \tag{3}$$

As shown in Fig. 11b, the approximate critical stress in (3) increases as $|C|$ decreases. The corresponding critical compressive stress in the transverse direction ($\sigma_{y,c} = C\sigma_{x,c}$) increases as well. As suggested by Fig. 9a, the stress ratio C in the end-clamped rectangular sheet decreases with the nominal strain for each aspect ratio. By comparing the critical compressive stress ($\sigma_{y,c}$) with the stretch-induced compressive stress (σ_y), we may predict qualitatively that stretch-induced wrinkles form at a critical nominal strain (ε_{c1}) when $\sigma_y = \sigma_{y,c}$. Subsequently, as the magnitude of σ_y increases and then decreases while the magnitude of $\sigma_{y,c}$ increases, a second critical nominal strain (ε_{c2}) may be predicted, beyond which the stretch-induced compressive stress drops below the critical stress. Therefore, stretch-induced wrinkles are expected only in between of the two critical strains ($\varepsilon_{c1} < \varepsilon < \varepsilon_{c2}$). Such a behavior is confirmed by the post-buckling analysis in Section 4.

As predicted by Eq. (3), the critical stress decreases as the sheet thickness (t) decreases. On the other hand, the stretch-induced compressive stress as shown in Fig. 9 is independent of the sheet thickness. By comparing the critical stress with the maximum magnitude of the stretch-induced compressive stress in Fig. 9b, we classify the sheet thickness into three types, as indicated by three dashed lines for the critical stresses. First, for a thick sheet, the critical stress is greater than the stretch-induced compressive stress for all aspect ratios. Thus, the thick sheet would not wrinkle upon stretching, regardless of the aspect ratio. Second, for a thin sheet, the stretch-induced compressive stress is greater than the critical stress for aspect ratios within a window ($\alpha_1 < \alpha < \alpha_2$). Third, for a very thin sheet, the stretch-induced compressive stress is greater than the critical stress for all aspect ratios beyond a critical value. The qualitative predictions based on the simplified model are confirmed by the post-buckling analysis for the cases of a thin sheet ($W_0/t_0 = 1000$) and a very thin sheet ($W_0/t_0 = 2000$) in Section 4.

Puntel et al. (2011) predicted a sequence of critical strains for increasing number of wrinkles. For a rectangular sheet with $W_0/t_0 = 1000$ and $L_0/W_0 = 2.5$, the minimum critical strain would be 4.5×10^{-6} by their prediction, which however is significantly lower than our numerical simulation (Fig. 14) and experimental observations (Zheng, 2009). The discrepancy is most likely due to the different boundary conditions assumed by Puntel et al. (2011) in their analysis.

4. Post-buckling analysis

To perform a post-buckling analysis of the end-clamped rectangular sheet, a small geometrical imperfection is introduced by using the eigenmodes from the eigenvalue analysis in Section 3. The numerical results in general depend on the number of eigenmodes and their amplitudes used as the geometrical imperfection (Nayyar, 2010). For the purpose of convergence, a sufficiently large number of eigenmodes and a sufficiently small amplitude must be used. In the present study, the first four eigenmodes are used for each sheet, and the amplitude of imperfection is about 0.1% of the sheet thickness. The RIKS method as implemented in ABAQUS is employed for the post-buckling analysis.

Fig. 12 shows evolution of stretch-induced wrinkles for a rectangular sheet with the aspect ratio $\alpha = 2.5$ and $W_0/t_0 = 1000$ as the nominal strain increases. Similar wrinkle patterns were observed in an experiment with polyethylene sheets (Fig. 1b); the details of the experiment and comparison with the numerical results will be reported in a subsequent work. The out-of-plane displacement (u_z) along the mid-section of the sheet ($x = L/2$) is plotted in Fig. 13. It is seen that the wrinkle amplitude grows significantly from $\varepsilon = 5\%$ to $\varepsilon = 10\%$. Subsequently, as the nominal strain increases further, the wrinkle amplitude decreases and eventually all wrinkles are nearly flattened at $\varepsilon = 30\%$. Similar results are obtained for different aspect ratios, as shown in Fig. 14 for the evolution of wrinkle amplitudes, where the amplitude is taken as $A = [\max(u_z) - \min(u_z)]/2$ from the numerical results. Such a wrinkling behavior is in drastic contrast with the scaling analysis by Cerda and Mahadevan (2003), which predicted the wrinkle amplitude to increase monotonically with increasing strain, i.e., $A \sim (Lt)^{1/2}\varepsilon^{1/4}$. On the other hand, as discussed in Section 3, by comparing the evolution of the stretch-induced compressive stress in Fig. 9a with the critical stress in Fig. 11b, the stretch-induced wrinkles are qualitatively predicted in between of two critical strains ($\varepsilon_{c1} < \varepsilon < \varepsilon_{c2}$) and hence non-monotonic scaling with the strain for the wrinkle amplitude. Fig. 14 shows that both critical strains depend on the aspect ratio of the sheet. Similar evolution of the wrinkle amplitude was predicted by Zheng (2009). By a dimensional consideration, the wrinkle amplitude may be written as

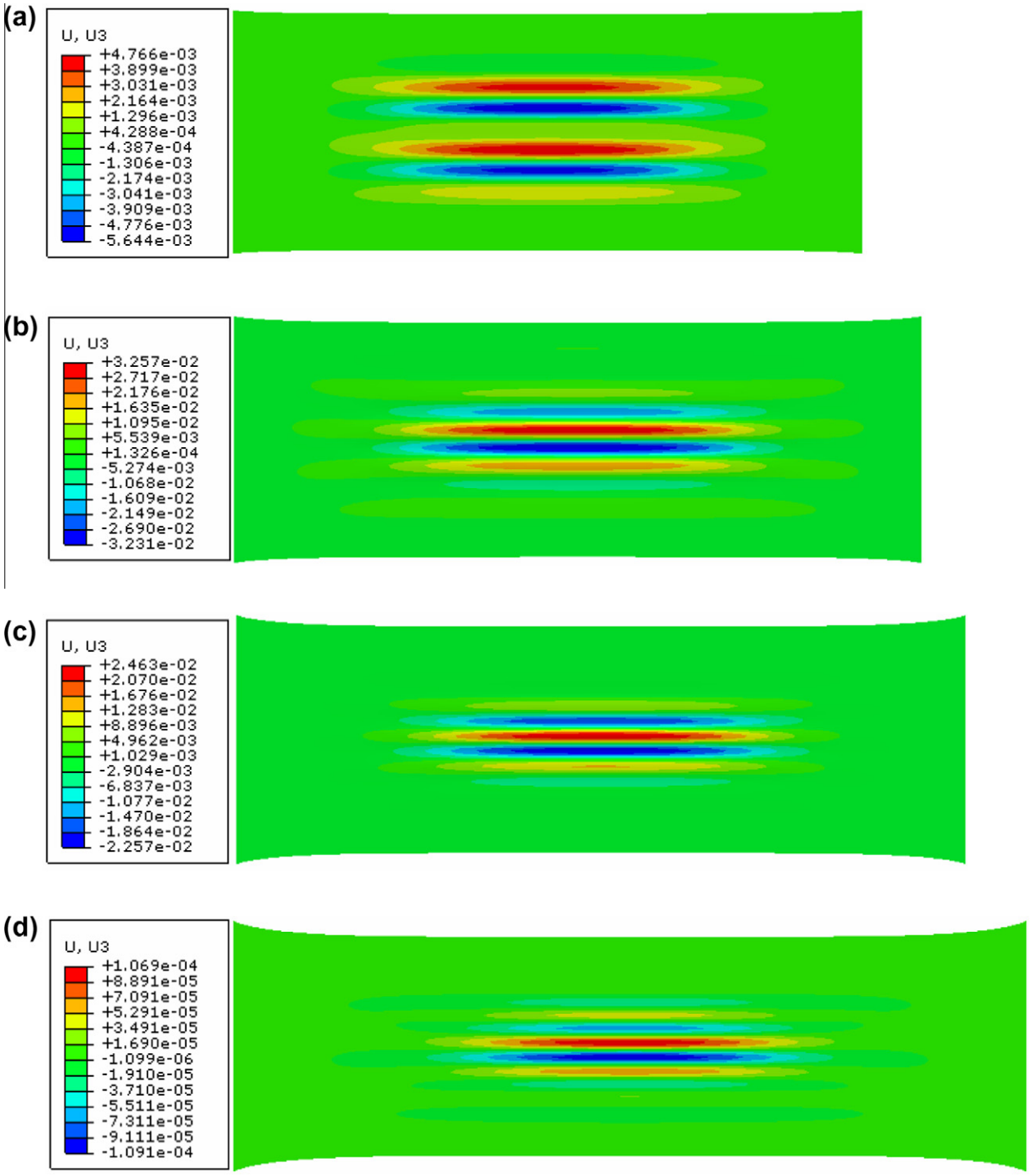

Fig. 12. Evolution of wrinkles in an end-clamped rectangular sheet with an aspect ratio $\alpha = 2.5$ and $W_0/t_0 = 1000$: (a) $\varepsilon = 5\%$; (b) $\varepsilon = 10\%$; (c) $\varepsilon = 20\%$; (d) $\varepsilon = 30\%$.

$$A/t_0 = f(\varepsilon, \alpha, W_0/t_0), \tag{4}$$

which is generally more complicated than the simple scaling relation. By using a different geometric constraint, Puntel et al. (2011) modified the scaling relation to include a multiplicative factor that depends on the strain and Poisson's ratio. However, the exact dependence on strain was not given explicitly, and the scaling with the sheet geometry (thickness and aspect ratio) remains the same as that by Cerda and Mahadevan (2003). As shown in Fig. 14, for the same width and thickness, the wrinkle amplitude first increases with the length and then decreases, with the maximum amplitude at $\alpha = 2.5$. In other words, the wrinkle amplitude does not increase monotonically with increasing length (L_0) of the sheet, again, in contrast with the scaling relation. We note that such a behavior may not be attributed simply to the nonlinear elastic material model used in the present study. The results are qualitatively similar if a linear elastic material model is used (Nayyar, 2010).

As shown in Fig. 12, the wrinkles are largely confined in the central region of the sheet where the transverse stress is compressive. However, the wrinkling region may not be exactly the region with the compressive stress by the 2-D stress analysis in Section 2 (Fig. 7 for $\alpha = 2.5$). As shown by Stein and Hedgepeth (1961), for a stretched membrane with a hub subject to torsion, the wrinkles could extend far beyond the compression region in a plate under

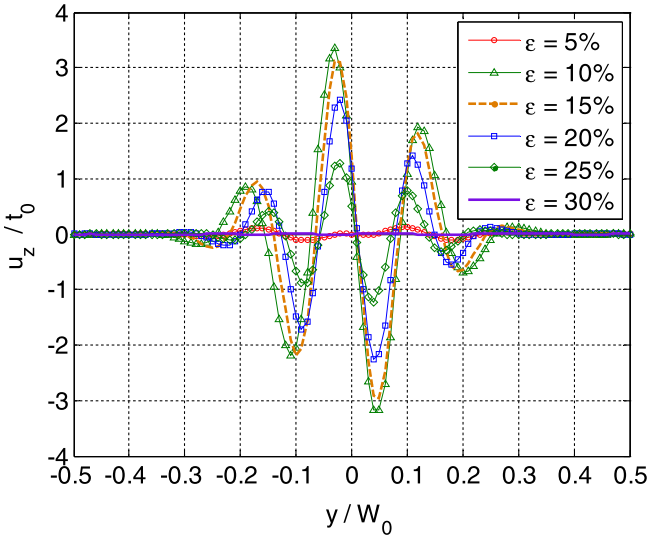

Fig. 13. Out-of-plane displacement along the mid-section of the sheet with $\alpha = 2.5$ and $W_0/t_0 = 1000$ under increasing nominal strain.

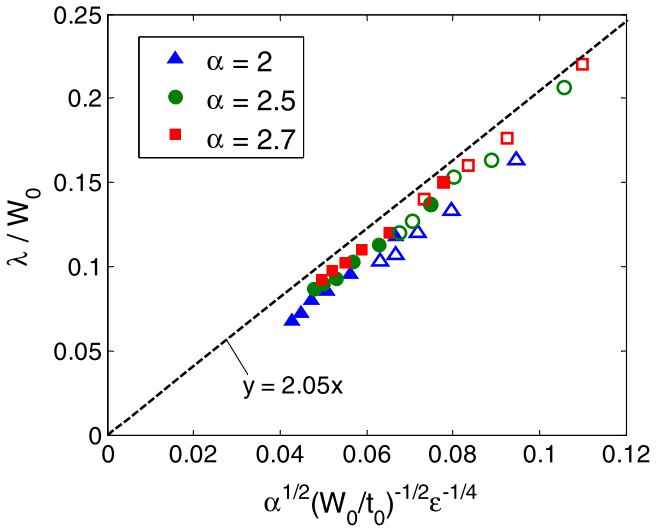

Fig. 15. Normalized wrinkle wavelength from the post-buckling analysis, in comparison with the prediction by a scaling analysis (dashed line). The open symbols show numerical results for $W_0/t_0 = 1000$, and the filled symbols for $W_0/t_0 = 2000$.

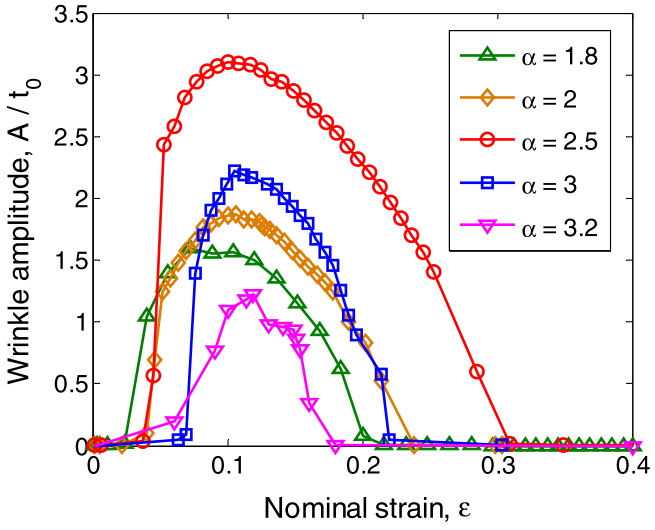

Fig. 14. Stretch-induced wrinkle amplitude as a function of the nominal strain for the end-clamped rectangular sheets with different aspect ratios. The width-to-thickness ratio (W_0/t_0) is 1000 for all cases.

same loading, which they attributed to the "over contraction" in the direction perpendicular to the wrinkling of the membrane. In the tension-field theory, the wrinkling region may be determined by replacing Poisson's ratio with an arbitrary function to result in a zero principal stress perpendicular to the wrinkles, rendering a different 2-D boundary value problem for the plate.

Fig. 13 shows that the sheet remains flat near the free edges and the wrinkling profiles are modulated by a long-wavelength mode, similar to the prediction by Puntel et al. (2011). However, we note that the number of wrinkles in the sheet remains nearly a constant, in contrast to the prediction by Puntel et al. (2011) that the number of wrinkles increases with increasing strain. On the other hand, the wrinkle wavelength, which may be measured from crest to crest, does decrease with increasing strain. The scaling analysis by Cerda and Mahadevan (2003) predicted that the wrinkle wavelength, $\lambda \sim (Lt)^{1/2}\varepsilon^{-1/4}$, or equivalently $\lambda/W \sim (L/W)^{1/2}(W/t)^{-1/2}\varepsilon^{-1/4}$ in a dimensionless form. Fig. 15 plots the normalized wrinkle wavelength (λ/W_0) versus $(L_0/W_0)^{1/2}(t_0/W_0)^{1/2}\varepsilon^{-1/4}$. Two sets of numerical results are presented in Fig. 15, for $W_0/t_0 = 1000$ (open symbols) and 2000 (filled symbols), respectively. For each set, the wavelengths are determined from the post-buckling analysis for three different aspect ratios ($\alpha = 2$, 2.5, and 2.7) and at different nominal strains. Evidently, the numerical results follow the prediction by the scaling analysis reasonably well; the latter is plotted as the dashed line with a slope depending on Poisson's ratio (taken to be 0.5 here). The experimental results reported by Cerda et al. (2002) also indicated that the wrinkle wavelength followed the scaling relation. It may thus be concluded that the scaling analysis offers a satisfactory prediction of the wrinkle wavelength, but less so for the wrinkle amplitude.

Furthermore, it is found that, for $W_0/t_0 = 1000$, the stretch-induced wrinkle amplitude is negligibly small for the sheets with the length-to-width aspect ratio smaller than 1.7 or larger than 3.5. Only when $1.7 < \alpha < 3.5$ is the stretch-induced compressive stress sufficiently large to cause wrinkling of the sheet. For each aspect ratio in this range, the lower and upper critical strains are determined from the post-buckling analysis, defining a wrinkling region in the $\alpha - \varepsilon$ plane, as shown in Fig. 16a. By decreasing the sheet thickness or increasing the ratio W_0/t_0, the critical stress for wrinkling drops and the wrinkling region in the $\alpha - \varepsilon$ plane expands. As shown in Fig. 16a for $W_0/t_0 = 2000$, the lower critical strain for onset of wrinkling is lower, whereas the upper critical strain for flattening is higher. Fig. 16b shows the maximum wrinkle amplitude as a function of the aspect ratio for $W_0/t_0 = 1000$ and 2000. Referring to the classification illustrated in Fig. 9b, the sheet with $W_0/t_0 = 1000$ is thin and the sheet with $W_0/t_0 = 2000$ is very thin. Therefore, for the latter case, stretch-induced wrinkling is predicted for $\alpha > 1.2$, with no upper bound for the aspect ratio of the sheet. In all cases, the wrinkling region in the $\alpha - \varepsilon$ plane is necessarily within the region of the stretch-induced compressive stress. The dashed line in Fig. 16a is the boundary between the regions with and without compressive stresses (Fig. 2).

We note in Fig. 16a that both the lower and upper critical strains depend on the in-plane aspect ratio of the sheet for $W_0/t_0 = 1000$. For $W_0/t_0 = 2000$, the lower critical strain is nearly independent of the aspect ratio, while the upper critical strain first increases and then decreases, eventually becoming independent of the aspect ratio for $\alpha > 5$. The dependence of the upper critical strain on the aspect ratio is similar to that of the maximum

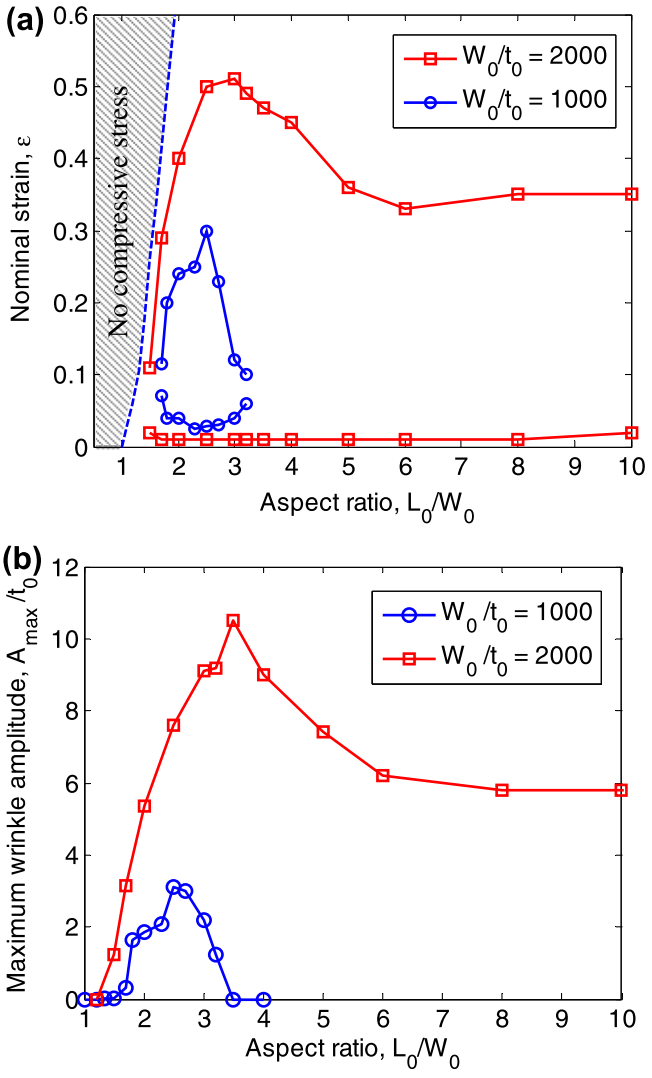

Fig. 16. (a) The wrinkling regions in the $\alpha - \varepsilon$ plane for two different width-to-thickness ratios. The dashed line is the boundary for the region with stretch-induced compressive stress (phases II-IV in Fig. 2); (b) The maximum wrinkle amplitude as a function of the aspect ratio.

compressive stress in Fig. 9b, and the dependence of the maximum wrinkle amplitude for the very thin sheets ($W_0/t_0 = 2000$) in Fig. 16b is similar too. The results shown in Fig. 16 suggest that stretch-induced wrinkling may be suppressed (1) by increasing the sheet thickness; (2) by designing the in-plane aspect ratio so that it is out of the wrinkling window in the case of a thin sheet; or (3) by stretching beyond the upper critical strain.

5. Summary

This paper presents a numerical study on stretch-induced wrinkling of hyperelastic rectangular sheets under uniaxial stretching with two clamped ends. As a prerequisite for wrinkling, a two-dimensional stress analysis is performed first under the plane-stress condition to determine stretch-induced compressive stresses in the transverse direction. Depending on the length-to-width aspect ratio of the sheet and the applied tensile strain, four different distribution patterns of the stretch-induced compressive stresses are predicted and summarized in a phase diagram. Next, eigenmodes of buckling are predicted by an eigenvalue analysis for pre-stretched sheets, which are used as geometric imperfections for the post-buckling analysis. A simplified plate model is adopted to estimate the critical condition for stretch-induced wrinkling, which qualitatively predicts wrinkling between two critical strains and the effect of sheet thickness. Finally, we examine the evolution of stretch-induced wrinkles by a nonlinear post-buckling analysis. It is found that the wrinkle wavelength decreases with increasing strain, in good agreement with the scaling analysis of Cerda and Mahadevan (2003). However, in contrast to the prediction of the scaling analysis, the wrinkle amplitude exhibits a non-monotonic dependence on the tensile strain with a lower critical tensile strain for onset of wrinkling and an upper critical tensile strain for wrinkle flattening. Based on the numerical results, it is suggested that stretch-induced wrinkling may be suppressed either by geometric design of the sheet (length-to-width aspect ratio and thickness) or by moderately large stretching beyond the upper critical strain. The numerical results reported in the present study will be compared to experimental measurements in a subsequent study.

Acknowledgments

VN and RH gratefully acknowledge financial supports by National Science Foundation (Grants Nos. 0547409 and 0926851).

References

ABAQUS, 2008. Theory and User's Manual, Version 6.8.
Alder, A.L., Mikulas, M.M., Hedgepeth, J.M., 2000. Static and dynamic analysis of partially wrinkled membrane structures. In: Proceedings of 41st AIAA/ASME/ASCE/AHS/ASC Structures, Structures Dynamics, and Material Conference and Exhibit. Atlanta. AIAA-2000-1810.
Benthem, J.P., 1963. A Laplace transform method for the solution of semi-infinite and finite strip problems in stress analysis. Q. J. Mech. Appl. Math. 16, 413–429.
Cerda, E., Mahadevan, L., 2003. Geometry and physics of wrinkling. Phys. Rev. Lett. 90, 074302.
Cerda, E., Ravi-Chandar, K., Mahadevan, L., 2002. Wrinkling of an elastic sheet under tension. Nature 419, 579–580.
Coman, C.D., 2007. On the applicability of tension field theory to a wrinkling instability problem. Acta Mech. 190, 57–72.
Coman, C.D., Haughton, D.M., 2006. Localized wrinkling instabilities in radially stretched annular thin films. Acta Mech. 185, 179–200.
Danielson, D.A., Natarajan, S., 1975. Tension field theory and the stress in stretched skin. J. Biomech. 8, 135–142.
Diaby, A., Le van, A., Wielgosz, C., 2006. Buckling and wrinkling of prestressed membranes. Finite Elem. Anal. Des. 42, 992–1001.
Friedl, N., Rammerstorfer, F.G., Fisher, F.D., 2000. Buckling of stretched strips. Comput. Struct. 78, 185–190.
Iwasa, T., Natori, M.C., Higuchi, K., 2004. Evaluation of tension field theory for wrinkling analysis with respect to the post-buckling study. J. Appl. Mech. 71, 532–540.
Jacques, N., Potier-Ferry, M., 2005. On mode localisation in tensile plate buckilng. C.R. Mec. 333, 804–809.
Jenkins, C.H., Haugen, F., Spicher, W.H., 1998. Experimental measurement of wrinkling in membranes undergoing planar deformation. Exp. Mech. 38, 147–152.
Lee, K., Lee, S.W., 2002. Analysis of gossamer space structures using assumed strain formulation solid shell elements. In: Proceedings of 43rd AIAA/ASME/ASCE/AHS/ASC Structures, Structural Dynamics and Materials Conference, Denver, Colorado. AIAA 2002-1559.
Leifer, J., Belvin, W.K., 2003. Prediction of wrinkle amplitudes in thin film membranes using finite element modeling. In: 44th AIAA/ASME/ASCE/AHS/ASC Structures, Structural Dynamics and Materials Conference, Norfolk, VA. AIAA 2003-1983.
Liu, X., Jenkins, C.H., Schur, W.W., 2001. Large deflection analysis of pneumatic envelopes using a penalty parameter modified material model. Finite Elem. Anal. Des. 37, 233–251.
Mansfield, E.H., 1970. Load transfer via a wrinkled membrane. Proc. Roy. Soc. Lond. A. 316, 269–289.
Nayyar, V., 2010. Stretch-Induced Compressive Stress and Wrinkling in Elastic Thin Sheets. Master's Thesis, Department of Aerospace Engineering & Engineering Mechanics, The University of Texas at Austin, Austin, TX.
Peypoudat, V., Defoort, B., Lancour, D., Brassier, P., Couls, O.L., Langlois, S., Lienard, S., Bernasconi, M., Gotz, M., 2005. Development of a 3.2m-long inflatable and rigidizable solar array breadboard. In: Proceedings of 46th AIAA/ASME/ASCE/AHS/ASC Structures, Structural Dynamics and Materials Conference, Austin, Texas. AIAA 2005-1881.
Pipkin, A.C., 1986. The relaxed energy density for isotropic elastic membrane. IMA J. Appl. Math. 36, 85–99.

Puntel, E., Deseri, L., Fried, E., 2011. Wrinkling of a stretched thin sheet. J. Elast. 105, 137–170.

Rogers, J.A. et al., 2001. Paper-like electronic displays: large-area rubber-stamped plastic sheets of electronics and microencapsulated electrophoretic inks. PNAS 98, 4835–4840.

Sakamoto, H., Park, K.C., 2005. Design parameters for wrinkle reduction in membrane space structures. In: Proceedings of 46th AIAA/ASME/ASCE/AHS/ASC Structures, Structural Dynamics and Materials Conference, Austin, Texas. AIAA 2005-1974.

Sleight, D.W., Michii, Y., Lichodziejewski, D., Derbes, B., Mann, T.O., Slade, K.N., Wang, J.T., 2005. Finite element analysis and test correlation of a 10-meter inflation-deployed solar sail. In: Proceedings of 46th AIAA/ASME/ASCE/AHS/ASC Structures, Structural Dynamics and Materials Conference, Austin, Texas. AIAA 2005-2121.

Steigmann, D.J., 1990. Tension-field theory. Proc. R. Soc. Lond. Ser. A, Math. Phys. Sci. 429, 141–173.

Steigmann, D.J., 2008. Two-dimensional models for the combined bending and stretching of plates and shells based on three-dimensional linear elasticity. Int. J. Eng. Sci. 46, 654–676.

Stein, M., Hedgepeth, J.M., 1961. Analysis of partly wrinkled membranes. NASA TN, D-813.

Su, X., Abdi, F., Taleghani, B., Blandino, J.R., 2003. Wrinkling analysis of a Kapton square membrane under tensile loading. In: Proceedings of 44th AIAA/ASME/ASCE/AHS/ASC Structures, Structural Dynamics and Materials Conference, Norfolk, VA. AIAA 2003-1985.

Talley, C., Clayton, W., Gierow, P., McGee, J., Moore, J., 2002. Advanced membrane materials for improved solar sail capabilities. In: Proceedings of 43rd AIAA/ASME/ASCE/AHS/ASC Structures, Structural Dynamics and Materials Conference, Denver, Colorado. AIAA 2002-1561.

Tessler, A., Sleight, D.W., Wang, J.T., 2005. Effective modeling and nonlinear shell analysis of thin membranes exhibiting structural wrinkling. J. Spacecr. Rockets 42, 287–298.

Timoshenko, S.P., Gere, J.M., 1985. Theory of Elastic Stability. McGraw-Hill.

Tomita, Y., Shindo, A., 1988. Onset and growth of wrinkling in thin square plate subjected to diagonal tension. Int. J. Mech. Sci. 30, 921–931.

Wagner, H., 1929. Flat sheet metal girder with very thin metal web. Zeitschrift fur Flugtechnik und Motorluftschiffahrt 20, 200–314.

Wang, X., Zheng, W., Hu, Y.R., 2007. Active flatness control of membrane structures using adaptive genetic algorithm. In: Proceedings of SPIE, vol. 6572, 652704.

Wong, Y.W., Pellegrino, S., 2006a. Wrinkled membranes. Part I: Experiments. J. Mech. Mater. Struct. 1, 1–23.

Wong, Y.W., Pellegrino, S., 2006b. Wrinkled membranes. Part II: Analytical models. J. Mech. Mater. Struct. 1, 25–59.

Wong, Y.W., Pellegrino, S., 2006c. Wrinkled membranes. Part III: Numerical simulations. J. Mech. Mater. Struct. 1, 61–93.

Wu, C.H., 1978. Nonlinear wrinkling of nonlinear membranes of revolution. J. Appl. Mech. 45, 533–538.

Zheng, L., 2009. Wrinkling of Dielectric Elastomer Membranes. PhD Thesis, California Institute of Technology, Pasadena, CA.